Exp. Theo. NANOTECHNOLOGY 10 (2026) 427-439 https://doi.org/10.56053/10.2.427

Wear rate, surface temperature, and nanoscaled tribo film formation in A319 and brass due to rotational speed

Aysha Sh. Hasan[1,2,], Mustafa N. Taifor[3], Nawzad J. Mahmood[4], Beyza Gavcar[2]*

[1]Department of Technical Renewable Energy, Northern Technical University, 36001 Kirkuk, Iraq
[2]Department of Mechanical Engineering, Yildiz Technical University, Beşiktaş,34220 Istanbul, Turkiye
[3]Renewable Energy Research Canter, Northern Technical University, 36001 Kirkuk, Iraq
[4]Imam Ja'afar Al-Sadiq University, Kirkuk 36001, Iraq
[*]) Email: eng_aysha@yahoo.com

Received 5/1/2026, *Received in revised form* 29/2/2026, *Accepted* 15/3/2026, *Published* 15/4/2026

This study utilizes an ASTM G99 pin-on-disc tribometer to examine how rotational speed affects the wear behaviour and surface temperature of aluminum alloy 319 (A319) and brass under dry sliding circumstances. The studies are done at room temperature with 0.5 kg of load and 1000–1400 rpm rotating speeds. Materials' tribological reactions are assessed by measuring wear rate and surface temperature. The two metals show opposing tendencies. Rotational speed increased brass wear due to frictional heating and the disintegration of nanoscale protective oxide layers. Nanoparticles generate during sliding contact detach faster, weakening and wearing the surface. The wear rate of aluminum alloy 319 decreases with higher rotational speed due to the creation of a thick Al_2O_3 tribo layer with nanoscale nanoparticles, acting as a protective barrier. Small oxide nanoparticles stabilize surfaces and reduce metal-to-metal contact. Increased heat conductivity in A319 decreases surface softening. Oxidative and abrasive wear processes create and remove nanoscale particles while sliding, as have shown by optical microscopy grooves, oxide coatings, and microcracks. By affecting wear response through thermal mechanical interactions and nanoparticle generation, rotational speed can optimize operating parameters and material selection for high-speed mechanical applications.

Keywords: Aluminum alloy 319; Brass; Nanoparticles; Rotational speed; Wear.

1. INTRODUCTION

Mechanical system efficiency, reliability, and longevity depend on friction and wear. When gears, bearings, shafts, and valves move relative to each other, contact interactions degrade surfaces and lose energy. Minimizing wear and friction is a top objective in modern engineering, especially in automotive, aerospace, and additive manufacturing, to enhance performance and sustainability [1,2]. Wear is material loss from a solid surface interacting with another. Nanoparticles result from frictional heating, severe plastic deformation, and contact surface oxidation. A complex interaction of sliding speed, applied tension, surface roughness, environment, and temperature causes wear. Sliding nanoparticles can form oxide layers or tribo-films, altering friction and wear [3,4]. Abrasive wear, when strong asperities or particles low or slash softer surfaces, causes roughly 50% of industrial wear failures [5–7].

Tribology research has moved from metallic to composite and additively made materials to study how operational factors affect wear processes. For instance, Tasci [5] has demonstrated that wear resistance in aluminum matrix composites varies significantly with speed-induced temperature changes and tribo-layer formation. Similarly, Taşcı et al. [8] have shown that hybrid Fe_3O_4-GNP reinforcement has improved the wear resistance of AA7020 alloys through microstructural stabilization at high sliding velocities. Tian et al. [9] have examined by putting up a model that connect noise, wear volume, and coefficient of fiction (COF). Under varied weights and speeds, ball-on-disc tribometer tests are performed on 304 stainless steel, UNS C38500 brass, and 6082 aluminum. They discover that whereas thermal expansion has a minor effect on brass and steel, it influences wear in aluminum. Wider use is indicated by the aluminum-based equation, which also predicts noise for brass and steel with errors of about 10% for 5-15 N loads and 0.21-0.63 m/s speeds. With the help of this model, friction, wear, and noise may be linked more simply, perhaps leading to advancements in mechanical systems' wear monitoring and noise management. Chen et al. [10] have described a method whereby cycles of detachment and reattachment at the contact interface are caused by periodic contact loss caused by reciprocating sliding motion. It has been demonstrated that the primary cause of friction-induced vibration and brake squeal is periodic impulsive excitation rather than mode-coupling. However, because these models do not account for wear-induced changes in surface morphology, their applicability in scenarios where wear is a major problem is restricted.

The impact of production parameters on tribological performance has been demonstrated by recent study on additive manufacturing. According to Gavcar et al. [9], they have found that geometric anisotropy induces during printing can alter wear behaviour, demonstrating the susceptibility of tribological performance to processing circumstances. These results provide credence to the notion that, independent of material type, wear processes are influenced by temperature, surface form, and structural alignment. In conventional metallic materials, frictional heat generation, surface temperature, oxidation, and material loss are all significantly influenced by rotational or sliding speed [11,12]. Although aluminum alloys like A319 are well-liked for their strength-to-weight ratio, machinability, and resistance to corrosion, brass is still utilized for bearings and bushings due to its ductility and conductivity. Under dynamic contact, their wear behaviours vary significantly. Brass creates less stable CuO/ZnO oxides that may separate during sliding, increasing material loss, whereas aluminum alloys produce a solid AlO_3 layer that decreases wear at high temperatures [13]. Thermo-mechanical coupling effects frictional heat production, contact stresses, and material deformation strongly affect sliding interface tribology. These combined processes greatly impact sliding contact wear mechanisms, oxide layer development, and surface microstructural evolution. Temperature increases and stress distribution at the contact interface affect protective tribo-film stability and wear resistance during dynamic loading [14].

Frictional heat and plastic deformation during dry sliding wear produce nanoparticle-based oxide layers at the contact surface. These small particles form protective tribo-films that reduce metal-to-metal contact, influencing sliding materials' tribology. Nanostructured oxide layer stability and distribution considerably affect friction, surface temperature, and sliding wear resistance. Nanoparticle formation and development during wear must be understood to improve high-speed mechanical material performance. Despite various research on aluminum copper alloy tribology, few have explicitly examined how rotational speed affects wear rate and surface temperature for A319 aluminum alloy and brass under comparable testing conditions. Predicting these materials' high-speed performance requires understanding rotational speed's influence on mechanical (slide distance) and thermal (interface temperature) effects.

Thus, this study examines how rotational speed affects wear and surface temperature of aluminum alloy 319 and brass in dry sliding circumstances. This study investigates the effects of rotational speed on thermal responses such as frictional heat production and interfacial temperature rise, as well as mechanical properties such as sliding distance and plastic deformation behaviour. Using an ASTM G99 pin-on-disc tribometer, the tribological performance of brass and aluminum alloy A319 is systematically examined at 1000–1400 rpm while under continuous loading. The creation and stability of nanoparticle-based tribo-oxide layers during sliding contact, as well as their impact on wear resistance and surface temperature evolution, are the main topics of discussion. In addition to helping with material selection and operational optimization in high-speed tribological applications, these investigations aim to provide light on thermo-mechanical wear mechanisms. Sliding interface tribology is significantly impacted by thermo-mechanical coupling effects, which include frictional heat generation, contact tensions, and material deformation. The growth of oxide layers, surface microstructural evolution, and sliding contact wear mechanisms are all significantly impacted by these coupled processes. During dynamic loading, protective tribo-film stability and wear resistance are impacted by temperature rises and stress distribution at the contact interface.

2. EXPERIMENTAL

For this investigation, two bulk materials -A319 and brass- are used in order to compare their wear rate response and surface temperature under varying rotational speeds. The chemical compositions of each alloy are shown in Tables 1 and 2. Cylindrical specimens (10 mm × 50 mm) are prepared using a hand saw in accordance with ASTM G99-95 standard. Subsequently, surfaces are grounded and polished using silicon carbide sandpapers with grit sizes (240 ,1200,3000) to achieve a smooth finish, washed in alcohol and distilled water, and dried in a drying machine [15].

Table 1 Chemical composition for aluminum alloy (A319).

Sn%	Mn%	Fe%	Cu%	Zn%	Al%
1.43	0.53	0.33	2.87	0.05	94.82

Table 2 Chemical composition for brass.

Fe%	Ni%	Cu%	Zn%	Pb%
0.46	0.3	61	35.69	2.15

A pin-on-disc configuration is employed to determine abrasive wear resistance under repeatable conditions. The test apparatus follows guidelines of ISO 18535 [16]. A dedicated pin-on-disc machine is used, (Figure 1) with the test performed under ambient room temperature and relative humidity ranging between 40 % and 50 %. Under regulated laboratory circumstances at room temperature (22 ± 2 °C), all tribological tests are conducted to enhance repeatability and dependability. To guarantee measurement accuracy, the measuring devices are calibrated before testing per manufacturer standards. While disc samples are firmly fixed to remove vibration, pin samples are firmly positioned in the holder to ensure consistent contact and avoid misalignment during testing. All trials are conducted under dry sliding conditions without lubrication to ensure uniform evaluation of wear and friction. The results shown are averages for data repeatability and reliability, with each experimental condition being carried out three times. Each pin specimen is weighed before and after the test with a high-precision balance (accuracy 0.0001 g). A K-type thermocouple is used to measure the temperature resulting from friction between the pin and the disc [15]. Dry sliding can create nanoscale wear debris via frictional heating, plastic deformation, and oxidation at the contact interface. These nanoparticles may form nanoscale oxide layers that affect tribology [17]. The wear rate is evaluated from mass loss before and after each test:

$$\Delta W = W_i - W_f \quad (1)$$

The original mass of the material (mg) is W_i whereas the final mass after testing is W_f. To compute the sliding distance S (cm), the linear sliding speed and test time are used. Expressing the linear sliding speed V:

$$V = 2\pi rn \quad (2)$$

V = linear sliding speed (m/min), r = 0.05, r=0.05 m = worn track radius, and n = disc rotational speed (1000, 1100, 1200, and 1400 rev/min) under voltage vector regulator universal inverter control. A 10-minute test length is maintained [18].

$$S = Vt \quad (3)$$

S represents the sliding distance (m). For centimetre reporting, sliding distance is converted:

$$S(cm) = 100x(2\pi rnt) \quad (4)$$

In conclusion, the wear rate WR is computed using mass loss per unit sliding distance:

$$WR = \frac{\Delta W}{100x(2\pi rnt)} \quad (5)$$

where WR is the wear rate (mg.cm^{-1}), ΔW is the mass loss (mg), and S is the sliding distance (cm).

Prior to testing, specimen surfaces are finished to a fine polish to minimize effects of surface roughness on wear behaviour. Recent studies emphasize that initial surface state significantly influences tribological outcomes [15,19]. Following wear testing, the shape of the wear tracks, the presence of debris, oxide layers, and cracking features are evaluated by optical microscopy on the worn surfaces. This procedure is in line with modern methods for identifying wear mechanisms [16].

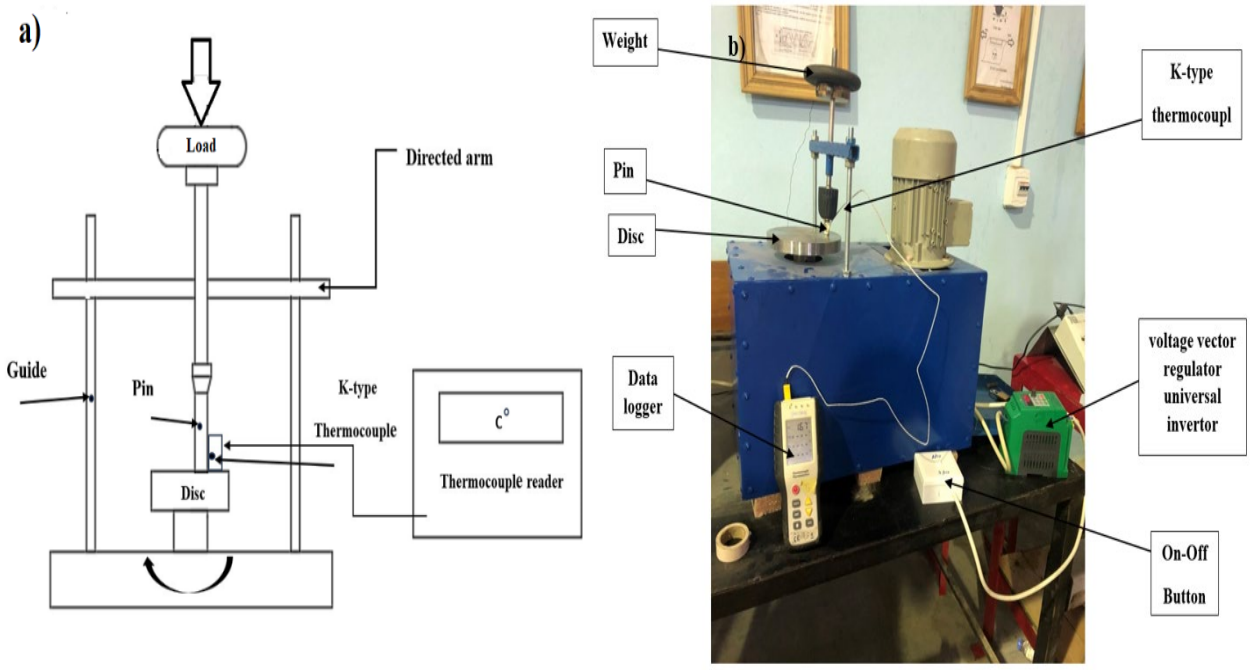

Figure 1 (a) Schematic of pin-on-disc test, (b) Pin-on-disc testing machine.

3. RESULTS AND DISCUSSION

Table 3 compares the current study to prior studies by Tasci [5], Taşcı et al. [8] and Tian et al. [9], emphasizing material, test technique, and tribological performance similarities and differences.

Table 3 Tribological performance comparison between current and prior research.

Study	Materials Investigated	Test Method and Conditions	Main Results	Similarities with the Present Study	Differences from the Present Study
Present Study	A319 aluminum alloy and brass	ASTM G99 dry sliding pin-on-disc tribometer; 0.5 kg load; 1000–1400 rpm	A319 alloy wear rate decreases with higher rotational speed because to stable Al_2O_3 tribo-oxide layer development, whereas brass wears more due to unstable oxide layers. Both materials' surface temperatures rose with speed	Shows how thermo-mechanical interaction and tribo-oxide layer development affect wear	Specifies dry sliding rotational speed effects and temperature progression
Tasci [5]	WS_2 and B_4C reinforced B319 aluminum matrix composite	Undergoes reciprocating wear testing in dry sliding circumstances	The optimal condition (2 wt% WS_2) lowered friction coefficient (0.497→0.178) and specific wear rate to 4.34×10^{-6} $mm^3/N\cdot m$, while improving hardness and TR	Both studies stress tribo-film development and nanoparticle impact on wear resistance	Tasci studied developed hybrid composites, whereas this work studies spontaneously generated oxide nanoparticles in A319 alloy and brass at different rotational speeds
Taşcı et al. [8]	Reinforced AA7020 alloy hybrid composites with 10 wt% Fe_3O_4 + 0.5–1% GNP	ASTM G99 pin-on-disc; load = 10 N; sliding speed = 1 m/s; 1500 m sliding distance; milling time 4–8 h.	Lowest specific wear rate: 7.86×10^{-7} $mm^3/N\cdot m$ (8 h, 1 wt% GNP); COF decreased to ~0.33 (from ~0.45); hardness raised to 149 HBN	ASTM G99 testing demonstrates hybrid particles/tribofilms minimize friction and wear	Parameters include reinforcing and milling time (microstructure control), not rotating speed or temperature.

Study	Materials Investigated	Test Method and Conditions	Main Results	Similarities with the Present Study	Differences from the Present Study
			and reducing friction.		
Tian et al. [9]	6082 Al, UNS C38500 brass, 304 stainless steel discs; 440C steel ball counter-face	Dry ball-on-disc (Anton Paar TRB3), loads 5–15 N, speeds 0.21–0.63 m/s, IR thermometer max temperature; FEM (COMSOL) + symbolic regression for noise–wear–COF model	Research highlighted noise as a wear monitoring output parameter	Emphasized wear,COF,noise interaction and FEM thermal modeling	Predicts wear. COF, noise using ball-on-disc testing and FEM simulation

3.1 Wear test

The variation of wear rate with rotational speed for brass and A319 samples is presented in Figure 2. For brass, the maximum wear rate is observed at 1400 rpm, while the minimum wear occurred at 1000 rpm. In contrast, A319 is exhibited an inverse trend, with wear rate decreasing as rotational speed increased. Table 4 summarizes the experimental results, including rotational speed, wear rate, and surface temperature of the samples.

Figure 2 shows the sample wear rate at different rotating speeds. The maximum brass wear rate is 1400 rpm, while the lowest is 1000. Conversely, rotational speed is decreased wear in A319. To ensure data dependability and reproducibility, the findings are the average of three separate trials, and the error bars display the standard deviation. At 1000 rpm, the wear rates are 6.03×10^{-9} mg/cm for brass and 6.38×10^{-9} mg/cm for A319 [20]. At 1400 rpm, brass wear rate reached 6.90×10^{-9} mg/cm, whereas A319 fell to 4.02×10^{-9} mg/cm. As rotating speed is increased, both materials' surface temperatures rose.

Table 4 Obtained data from rotational speed, rate of wear and temperature for samples.

Metal	Sample	Load kg	Rotational speed rev/min	Wear rate mg.cm-1	Temperature ºC
Brass	1	0.5	1000	6.03E-09	47
	2		1100	6.50E-09	52
	3		1200	6.60E-09	56
	4		1300	6.70E-09	62.5
	5		1400	6.90E-09	66
Aluminum	1		1000	6.38E-09	62
	2		1100	6.10E-09	69
	3		1200	5.67E-09	71
	4		1300	5.23E-09	86
	5		1400	4.02E-09	91

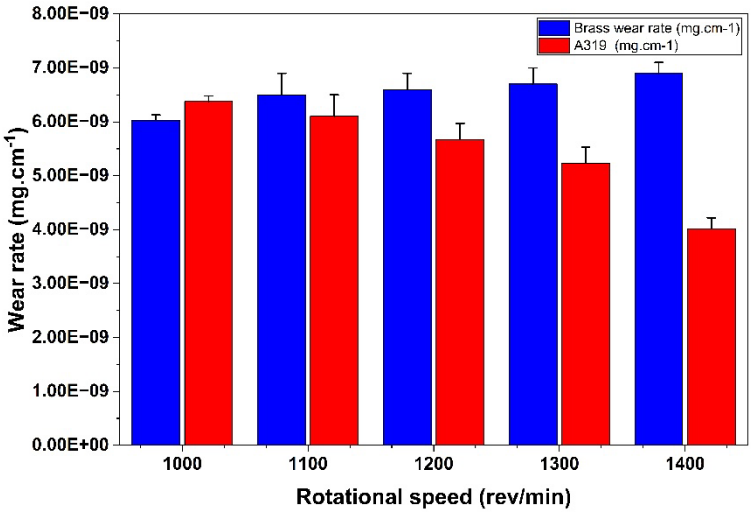

Figure 2 Rotational speed vs wear rate values for A319 and brass samples.

3.2 Wear mechanisms

Due to frictional heat generation at the contact surface, which intensifies thermo-mechanical interactions and limits heat dissipation, rotational speed causes an increase in brass wear [21]. This behaviour is significantly impacted by the mechanical and thermal differences between brass and A319 alloy. Because A319 has a slightly higher thermal conductivity (≈116 W/m·K) [22] than brass (≈109 W/m·K), there is less thermal softening at the sliding contact and improved frictional heat dissipation. A319's lower hardness (89.51 ± 5.6 HV) [23] and better ductility than brass (60 to 150 HV) [24] facilitate plastic

deformation while sliding. This deformation helps compress and consolidate oxide nanoparticles, forming a stable and adherent Al_2O_3 tribo-oxide layer. Brass is harder and less ductile, limiting plastic flow and oxide nanoparticle retention. Thus, oxide coatings on brass surfaces are less stable and more likely to dislodge during sliding.

Temperature increases oxidation kinetics and influences sliding tribo-oxide layer stability and thickness. Increased frictional heating causes oxide nanoparticles to develop and detach at the sliding surface, resulting in unstable protective layers and increased material loss [4]. At higher speeds, A319 exhibits increased wear resistance due to the creation of a protective Al_2O_3 oxide layer that minimizes metal-to-metal contact [25]. In this oxide layer, fine nanoparticles form a thick nanoscale tribo-film that resists wear. Frictional heating also softens aluminum locally, promoting plastic flow and lubricating tribolayer development, reducing wear [26]. High interfacial temperature enhances oxide nanoparticle sintering and consolidation, improving tribo-film continuity and load-bearing capability. Nanostructured tribo-layers stabilize sliding contact by repositioning nanoscale wear debris [27]. Brass creates CuO/ZnO oxides that are less adhering, readily removed, and insufficiently protective, causing wear at higher speeds [28]. Oxide nanoparticles on brass surfaces fracture and detach more quickly, reducing their ability to form stable nanoscale protective layers. Frictional heating also softens brass, promoting plastic deformation and subsurface cracking [29,30].

3.3 Topography analysis

The wear mechanism of the samples is analysed using an optical microscope (Euromax trinocular metallurgical microscope) at 50× magnification [31]. Figure 3 shows the morphology of the worn surfaces. Sliding direction is indicated by double-headed purple arrows, red circles denote oxide points, blue rectangles indicate longitudinal cracks, and green ellipses indicate transverse cracks. Figure 3b shows an enlarged area of the A319 friction surface.

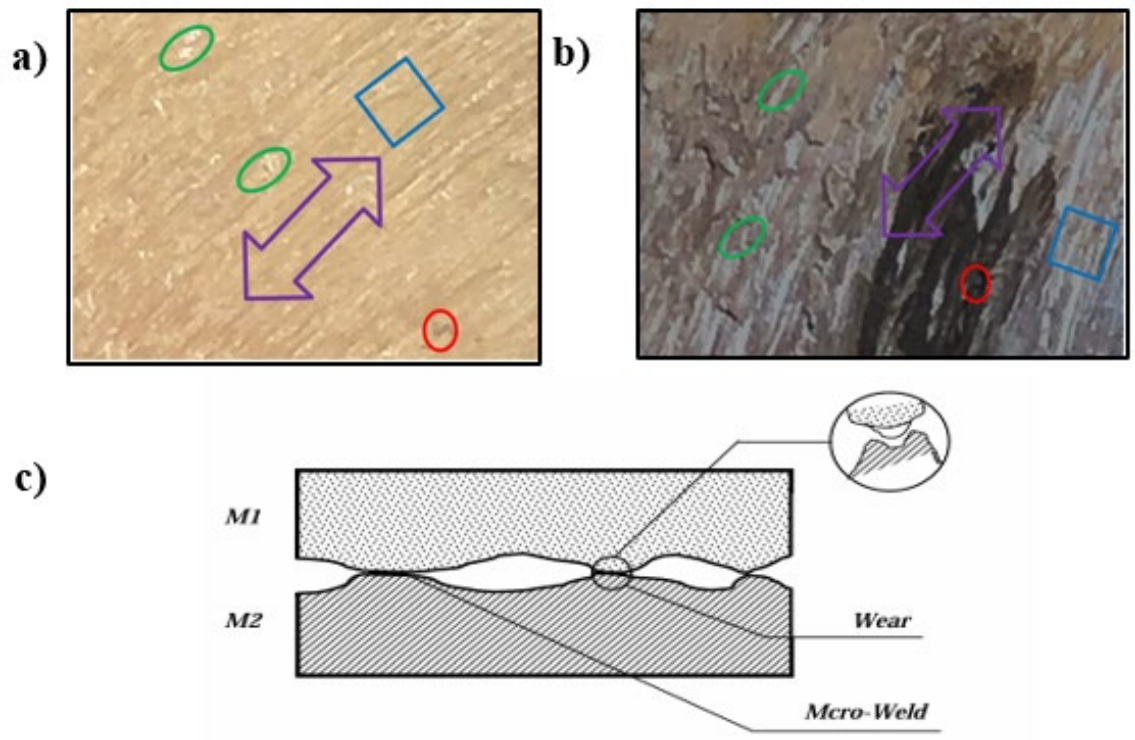

Figure 3 Morphology of worn surface with (magnification 50x), (a) For brass samples, (b) For A319 samples, (c) A schematic illustration of a debris mechanism.

Optical microscopy has revealed that both longitudinal and transverse cracks develop during wear, accompanied by metal debris formation and plastic flow of the worn surface [32]. Debris from mechanical wear and oxidation may be nanoparticle fragments. The difference in the levels of wear, as is known, to the difference in the two metals due to the difference in hardness and the difference in the plastic deformation of the two metals. A319 exhibits more plastic deformation than brass due to its lower hardness, which absorbs more energy and converts it to heat at the contact surface, facilitating abrasive wear [33–38]. The accelerated oxidation of A319 also contributes to the formation of a protective tribolayer [38]. This tribolayer may contain compact oxide nanoparticles for surface stability and wear reduction [27].

Increasing the rotational speed increases both friction and surface temperature, as has reflected in Figure 4b–c, supporting the trends that is observed in Figure 2 [39]. The abrasive wear mechanism is illustrated schematically in Figure 4a [40]. It is also observed from Figure 4 (b&c), increasing in the number of revolutions of the disc leads to increase in friction and temperature [41]. High temperatures may promote nanoparticle production and redistribution along the wear track, affecting tribology.

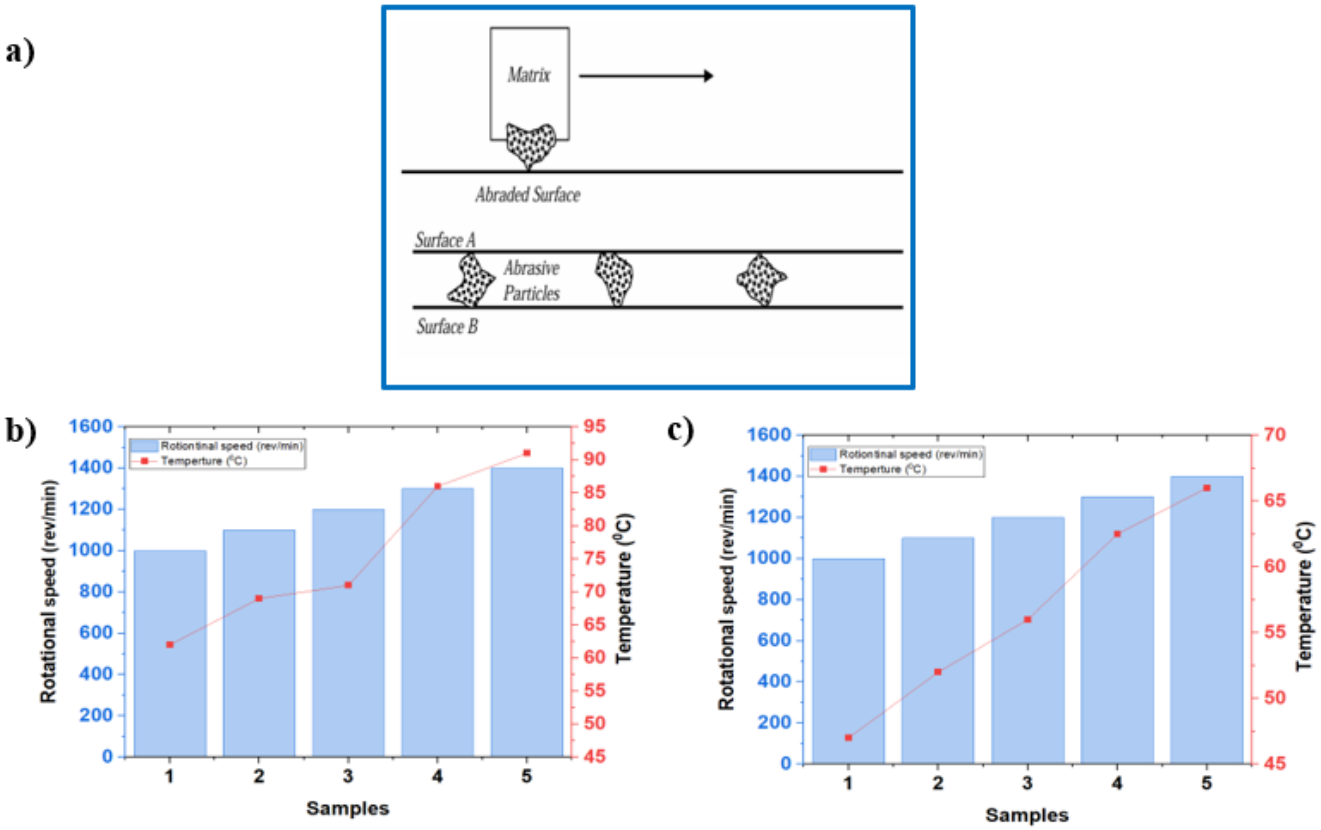

Figure 4 (a) A representation of abrasive-worn surfaces schematically, The relation between rotational speed and temperature for (b) Brass samples, (c) A319 samples.

4. CONCLUSIONS

Using a pin-on-disc configuration in compliance with ASTM G99, this study examines the impact of rotational speed on the wear behaviour and surface temperature of brass and aluminum alloy 319 in dry sliding conditions. The findings showed clear variations in the two materials' tribological performance, mainly due to their mechanical characteristics and propensity for oxide formation, during sliding contact,

tiny oxide particles form. For brass, the wear rate is increased with increasing rotational speed, indicating a direct correlation between speed, frictional heating, and material loss. Lack of a stable oxide layer makes brass more vulnerable to plastic deformation and subsurface cracking at higher speeds, accelerating wear. The oxide coatings on brass surfaces are likely unstable nanoparticles that quickly fractured and separated, reducing their protective efficacy. A319 shows a decrease in wear rate with higher rotating speed due to the quick creation of a protective Al_2O_3 tribo layer and a lubricating smearing layer at high sliding velocities. Tribo layers are hypothesized to be thick nanoscale protective films of compact oxide nanoparticles. Even at greater surface temperatures, this protective mechanism minimized metal-to-metal contact and material loss. Both materials showed longitudinal and transverse fissures, plastic flow, and wear debris under optical microscopy, although A319's lower hardness cause greater plastic deformation. Nanoscale wear debris may result from mechanical fragmentation and oxidation during sliding. The wear process is largely dependent on material type and operation speed, stressing the relevance of tribo layer development, oxide stability, and surface shape when selecting materials for high-speed mechanical applications. The study offers helpful suggestions for enhancing the longevity and performance of brass and aluminum components under high-speed conditions. Compared to brass, which can require surface treatments or lubrication, A319 is superior in circumstances where protective tribo-oxide formation can stop wear at high sliding speeds. Engineering-wise, A319 alloy is advised for high-speed bearing systems with stable tribo-oxide layer development to increase wear resistance and service life, lightweight rotating shafts, and automotive engine components. Because of their machinability and resistance to corrosion, brass components are widely used; however, surface engineering may be required in high-speed or high-friction environments. Oxide layer stability and wear resistance are increased by controlled oxidation treatments, hard coating deposition, and wear-resistant particle reinforcement. Additionally, proper lubrication can reduce oxide layer separation, frictional heating, and the durability of dynamic loading. Engineers should take into account oxide layer stability, thermal conductivity, material hardness, and thermo-mechanical operating conditions when choosing materials for high-speed tribological systems. This study suggests A319 alloy for dry sliding circumstances and high rotating speeds and provides helpful guidance for enhancing the performance and dependability of brass and aluminum components in high-speed mechanical applications.

References

[1] R. Mercado-Lemus, V. H., Gomez-Esparza, C. D., Díaz-Guillén, J. C., Mayén-Chaires, J., Gallegos-Melgar, A., Arcos-Gutierrez, H., Hernández-Hernández, M., Garduño, I. E., Betancourt-Cantera, J. A., & Perez-Bustamante, Metals (Basel) 11 (2021) 1652 https://doi.org/https://doi.org/10.3390/met11101652

[2] K.S. Hassan, Int. J. Eng. Technol. 4 (2015) 71 https://doi.org/10.14419/ijet.v4i1.3866

[3] S.B. Nagaraju, M.K. Somashekara, P.D. Govindaswamy, M. Puttegowda, P.B.G. Shankar, K. Sathyanarayana, J. Eng. Appl. Sci. 70 (2023) 124 https://doi.org/10.1186/s44147-023-00294-6

[4] K. Lontin, M.A. Khan, B. Alharbi, Materials (Basel). 15 (2022) 812 https://api.semanticscholar.org/CorpusID:246190291

[5] U. Tasci, Lubricants 13 (2025) 247 https://doi.org/10.3390/lubricants13060247

[6] J. Christ, M. Filips, S. Artois, R. Nowak, M. Reed, W. Knoll, Exp. Theo. NANOTECHNOLOGY 7 (2023) 87 https://doi.org/10.56053/7.2.87

[7] S.A. Alnuaimi, D. Vaishnavi, H.G. Hameed, Exp. Theo. NANOTECHNOLOGY 9 (2025) 513 https://doi.org/10.56053/9.3.513

[8] U. Taşcı, T.A. Yılmaz, H. Karakoç, Ş. Karabulut, Lubricants 12 (2024) 215 https://doi.org/10.3390/lubricants12060215

[9] Y. Tian, M. Khan, H. Deng, I. Omar, Tribol. Int. 203 (2025) 110403 https://doi.org/10.1016/j.triboint.2024.110403

[10] F. Chen, H. Ouyang, X. Wang, Friction 11 (2023) 302 https://doi.org/10.1007/s40544-022-0602-0

[11] B. Gavcar, E.H. Sumer, B. Sagbas, J.K. Katiyar, Proc. Inst. Mech. Eng. Part J J. Eng. Tribol. 237 (2023) 2213 https://doi.org/10.1177/13506501231209396
[12] E. Mohan, G. Anbuchezhiyan, R. Pugazhenthi, F.P. Prakash, Mater. Res. 26 (2023) 196 https://doi.org/10.1590/1980-5373-MR-2022-0196
[13] M.A. Chowdhury, IntechOpen, London, 2019 https://doi.org/10.5772/intechopen.77584
[14] L. Shi, X. Li, H. Gao, Y. Liu, J. Yin, S. Zhang, Z. Sha, Tribol. Int. 214 (2026) 111287 https://doi.org/https://doi.org/10.1016/j.triboint.2025.111287
[15] ASTM. International, ASTM G99-95: Standard Test Method for Wear Testing with a Pin-on-Disk Apparatus, West Conshohocken, PA, USA, 2020
[16] ISO. 18535:2020, Wear Test Methods for Materials—Pin-on-Disk Method, Geneva, Switzerland, 2020
[17] G.P. Alparone, D. Penney, E. Jewell, J. Sullivan, C. Mills, Mater. (Basel, Switzerland) 16 (2023) 7252 https://doi.org/10.3390/ma16237252
[18] ASTM International, Standard Test Method for Wear and Friction Testing with a Pin-on-Disk or Ball-on-Disk, (2023) 99 https://doi.org/10.1520/G0099-23
[19] I. Barányi, Acta Tech. Jaurinensis 13 (2020) 151 https://doi.org/10.14513/actatechjaur.v13.n2.542
[20] F. F. S. Al-Enzi, S. S. Mohammed, Eng. Res. J. - Fac. Eng. 46 (2020) 16 https://doi.org/10.21608/erjsh.2020.228172.
[21] R.V. Marode, T.A. Lemma, S.R. Pedapati, S. Kusekar, V.D. Birajdar, A. Hassan, Lubricants 13 (2025) 450 https://doi.org/10.3390/lubricants13100450
[22] S.I. Bakhtiyarov, R.A. Overfelt, S.G. Teodorescu, J. Mater. Sci. 36 (2001) 4643 https://doi.org/10.1023/A:1017946130966
[23] T.K. Akopyan, N.A. Belov, A.A. Lukyanchuk, N. V Letyagin, F.O. Milovich, A.S. Fortuna, J. Alloys Compd. 921 (2022) 166109 https://doi.org/https://doi.org/10.1016/j.jallcom.2022.166109
[24] S. Jasper, R. Subash, K. Muthuneelakandan, D. Vijayakumar, S. Jhansi Ida, Eng. Proc. 93 (2025) 11 https://doi.org/10.3390/engproc2025093011
[25] H. Yantao, L. Guodong, L. Yutao, J. Xiaoliang, W. Kaiming, Y. Xiaojun, L. Jian, F J. Mater. Sci. 60 (2025) 17608 https://doi.org/10.1007/s10853-025-11549-3
[26] P. Huang, X. Chen, W. Deng, J. Luo, Mater. Today 92 (2026) 552 https://doi.org/https://doi.org/10.1016/j.mattod.2025.11.026.
[27] D. Maharaj, B. Bhushan, Beilstein J. Nanotechnol. 3 (2012) 759 https://doi.org/10.3762/bjnano.3.85
[28] Hussian Fakhry, Mohammed RASHEED, Odai N. Salman, Raid A. Ismail, Exp. Theo. NANOTECHNOLOGY 10 (2026) 81 https://doi.org/10.56053/10.1.81
[29] L. Qiao, B. Zhou, R. Li, T. Li, Y. Zhao, X. Zhang, C.-H. Lee, Lubricants 13 (2025) 10 https://doi.org/10.3390/lubricants13010010
[30] W. Smith, A. Becker, L. Harison, Exp. Theo. NANOTECHNOLOGY 4 (2020) 189 https://doi.org/10.56053/4.3.189
[31] Wedyan G. Nassif, Nadia M. Abed, Ruaa M. Ibrahim, Amal Jaafar Salim Al-Azawee, Osama T. Al-Taai, Exp. Theo. NANOTECHNOLOGY 10 (2026) 153 https://doi.org/10.56053/10.1.153
[32] J.-L. Rebière, M.-N. Maâtallah, D. Gamby, Compos. Struct. 53 (2001) 173 https://doi.org/https://doi.org/10.1016/S0263-8223(01)00002-2.
[33] Ş. Taşcı, U.; Yılmaz, T.A.; Karakoç, H.; Karabulut, Lubricants 12 (2024) 215 https://doi.org/10.3390/lubricants12060215
[34] V. Singhal, D. Shelly, A. Babbar, S.-Y. Lee, S.-J. Park, Lubricants 12 (2024) 350 https://doi.org/10.3390/lubricants12100350.
[35] N.J. Mahmood, A.A. Hussein, A.S. Hasan, O.M. Ali, Ann. Chim. Sci. Des Mater. 46 (2022) 247 https://doi.org/10.18280/acsm.460503
[36] S. Jasper, R. Subash, K. Muthuneelakandan, D. Vijayakumar, S. Jhansi Ida, Eng. Proc. 93 (2025) 11 https://doi.org/10.3390/engproc2025093011.

[37] N. J.Mahmod, A.S. Hasan, A.A. Hussein, O.M. Ali, Int. J. Eng. Technol. 7 (2018) 214 https://doi.org/10.14419/ijet.v7i4.37.24104
[38] L. da Conceição, A.S.C.M. D'Oliveira, Surf. Coatings Technol. 288 (2016) 69 https://doi.org/https://doi.org/10.1016/j.surfcoat.2016.01.013
[39] B. Sugito, A.D. Anggono, A.S. Darmawan, A. Hariyanto, Eng. Proc. 84 (2025) 15 https://doi.org/10.3390/engproc2025084015
[40] M.R. da Silva, V.T. dos Santos, F.G. Lobo, D.A. Seixas, I.F. Machado, Appl. Sci. 14 (2024) 6001 https://doi.org/10.3390/app14146001
[41] J. Verma, L. Nagdeve, H. Kumar, Proc. Inst. Mech. Eng. Part E J. Process Mech. Eng. 236 (2022) 178 https://doi.org/10.1177/09544089211042954